Electron-hole balance and the anomalous pressure-dependent superconductivity in black phosphorus

Jing Guo, Honghong Wang, Fabian von Rohr, Wei Yi, Yazhou Zhou, Zhe Wang, Shu Cai, Shan Zhang, Xiaodong Li, Yanchun Li, Jing Liu, Ke Yang, Aiguo Li, Sheng Jiang, Qi Wu, Tao Xiang, Robert J. Cava, and Liling Sun

Phys. Rev. B **96**, 224513 — Published 27 December 2017

DOI: 10.1103/PhysRevB.96.224513

Electron-hole balance and the anomalous pressure-dependent superconductivity in black phosphorus

Jing Guo[1]*, Honghong Wang[1,5]*, Fabian von Rohr[2], Wei Yi[1], Yazhou Zhou[1,5], Zhe Wang[1,5], Shu Cai[1,5], Shan Zhang[1,5], Xiaodong Li[3], Yanchun Li[3], Jing Liu[3], Ke Yang[4], Aiguo Li[4], Sheng Jiang[4], Qi Wu[1], Tao Xiang[1,5,6], Robert J Cava[2], Liling Sun[1,5,6]†

[1]*Institute of Physics and Beijing National Laboratory for Condensed Matter Physics, Chinese Academy of Sciences, Beijing 100190, China*

[2]*Department of Chemistry, Princeton University, Princeton, New Jersey 08544, USA*

[3]*Institute of High Energy Physics, Chinese Academy of Science, Beijing 100049, China*

[4]*Shanghai Synchrotron Radiation Facilities, Shanghai Institute of Applied Physics, Chinese Academy of Sciences, Shanghai 201204, China*

[5]*University of Chinese Academy of Sciences, Beijing 100190, China*

[6]*Collaborative Innovation Center of Quantum Matter, Beijing, 100190, China*

Here we report the first *in-situ* high pressure (up to ~ 50 GPa) Hall effect measurements on single crystal black phosphorus. We find a strong correlation between the sign of the Hall coefficient, an indicator of the dominant carrier type, and the superconducting transition temperature (T_C). Importantly, we find a change from electron-dominant to hole-dominant carriers in the simple cubic phase of phosphorus at a pressure of ~17.2 GPa, providing an explanation for the puzzling valley it displays in its superconducting T_C vs. pressure phase diagram. Our results reveal that hole-carriers play an important role in developing superconductivity in elemental phosphorus, and the valley in T_C at 18.8 GPa is associated with a Lifshitz transition.

PACS number: 72.80.Cw, 74.25.Fy, 74.62.Fj

Black phosphorus is an archetypical band semiconductor, regarded as an analog of graphite [1], and its monolayer variant phosphorene is similar to graphene [2-4]. Recently, the electronic topological transition found in the orthorhombic semiconducting phase at 1.2 GPa [5-9] has made black phosphorus a new focus of research in condensed matter physics and material science. Bulk black phosphorus single crystals display high charge mobility [10] and thin film black phosphorus single crystals exhibit drain current modulation and high mobility [11, 12], suggesting potential applications in electronic and optoelectronic devices.

Structurally, bulk black phosphorus crystallizes in an orthorhombic structure with buckled layers bonded to each other by van der Waals forces. Because pressure can shrink the volume of solids, alter atomic distances, modify chemical bonds or even induce structural phase transitions, it can often modify electronic properties significantly [13-18]. Indeed, black phosphorus presents two pressure-induced crystal structure transitions, first from an orthorhombic (O) phase to a rhombohedral (R) phase at ~5 GPa, and then to a simple cubic (C) phase at ~12 GPa [19-24]. These phases display a diversity of physical properties, in particular superconductivity in both the R and C forms [25-28]. Intriguingly, black phosphorus shows a puzzling valley in its superconducting T_C versus pressure behavior within the cubic phase region of the P-T_C phase diagram [25]. A unified understanding for the complex superconducting behavior in elemental phosphorus remains lacking.

The influence of carrier type on superconductivity is an important issue for both conventional and unconventional superconductors [29-35]. Although hole-carriers

were proposed to play a role in developing superconductivity for elemental metals [36-39], their role in elements that are not normally conducting but can be converted to superconductors remains unclear due to the lack of experimental data. In this study, we report the results of a suite of complementary high-pressure measurements, with the aim of revealing the correlation between superconducting transition temperature (T_C) and Hall coefficient in the different structural phases of pressurized black phosphorus, while detailing the superconductivity-structure-pressure phase diagram of this normally semiconducting element.

Large, high-quality crystals of black phosphorus were obtained by a vapor transport technique [40]. Dry red phosphorus (150 mg, purity 99.99%), dry SnI_4 (10 mg, purity 99.999%), tin shot (40 mg, purity 99.8 %), and gold shot (20 mg, purity 99.999 %) were sealed in an evacuated quartz glass tube. The mixture was heated to 680 °C and held at this temperature for 10 h. It was then cooled with 0.1 K/h to 500 °C, and quenched to room temperature.

Pressure was generated by a diamond anvil cell with two opposing anvils sitting on Be-Cu supporting plates. Diamond anvils with 300 μm flats and non-magnetic rhenium gaskets with 100 μm diameter holes were employed for different runs of the high-pressure studies. The four-probe method was applied on the *ab* plane of single crystal black phosphorus for the high-pressure resistance measurements [41]. In these measurements, insulation from the rhenium gasket was achieved by a thin layer of a mixture of c-BN powder and epoxy. The four electrodes made by Pt foil were placed on the insulating layer, following by put the single crystal sample on the top of the

electrodes. In the high pressure Hall effect measurements, the Van der Pauw method [42] was used (See Supplemental Information). To keep the sample in a quasi-hydrostatic pressure environment, NaCl powder was employed as a pressure transmitting medium for the resistance and Hall coefficient measurements. High-pressure alternating-current (*ac*) susceptibility measurements were conducted using home-made primary/secondary-compensated coils that were wound around a diamond anvil [43, 44]. The frequency used for the real part of the susceptibility data is 157 Hz. The balanced secondary coils are connected with a lock-in amplifier. The in-phase output signal from the secondary coils was recorded. Silicon oil was used as pressure medium in our *ac* susceptibility studies. Pressure in all measurements was determined by the ruby fluorescence method [45].

Ambient pressure and high pressure X-ray diffraction (XRD) measurements were carried out at beamline 4W2 at the Beijing Synchrotron Radiation Facility and at beamline 15U at the Shanghai Synchrotron Radiation Facility, respectively. Diamonds with low birefringence were selected for the X-ray experiments. A monochromatic X-ray beam with a wavelength of 0.6199 Å was employed. To maintain the sample in a hydrostatic pressure environment, silicon oil was used as a pressure transmitting medium. Pressure was also determined by the ruby fluorescence method [45].

The quality of the single crystal investigated in this study was examined through synchrotron x-ray diffraction (XRD) measurements. As shown in Fig.1a, all the peaks detected from the powdered sample obtained from ground single crystals can be well indexed in the orthorhombic structure in space group *Cmca*, in good agreement with

previous results [46]. Analysis of the crystals by scanning electron microscopy (SEM) demonstrates that the surfaces of the crystals are flat, and that the thickness of the samples employed lies in the 3μm -10μm range (inset of Fig.1a). The combined results obtained from our XRD and SEM experiments indicate that the single crystals used for the present study are of high quality.

High pressure X-ray diffraction (XRD) measurements show that black phosphorus undergoes two structural phase transitions at high pressure. At around 5 GPa the orthorhombic (O) phase partially transforms to a rhombohedral (R) phase that coexists with the O phase between 5 and 8.7 GPa and then becomes a single phase at higher pressure. Finally, the R phase converts to the simple cubic (C) phase at 12.4 GPa. The compressibility in the C phase changes smoothly and continuously with pressure up to 35 GPa (Fig.1b-1f). This C phase can be stabilized under pressure up to 100 GPa [23]. The pressure-induced crystal structure transitions are also confirmed by our high-pressure Raman measurements, which show that the Raman modes change at the pressure of the structural phase transitions (Fig.S1 of the Supplementary Material [47]).

Figure2a–2d display the temperature dependence of the electrical resistance at different pressures. It is seen that a semiconductor-to-metal transition occurs at 2.3 GPa (Fig.2a). Upon increasing the pressure to 4.9 GPa, a resistance drop, characteristic of superconductivity, is found at ~3.2 K (Fig.2b), which shifts to higher temperature with increasing pressure. Zero resistance is attained at pressures higher than 9.6 GPa. The onset temperature of the superconducting transition exhibits an anomalous evolution with increasing pressure (Fig.2c and Fig.2d) intriguingly exhibiting a minimum at a pressure of ~18.8 GPa (Fig.2c and inset). We also observed this unusual evolution of the resistance-temperature-pressure behavior in an

independent measurement (Fig.S4 of the Supplementary Material [47]), and it has also been detected by another group [25]. To confirm that the resistance drop detected in the pressurized black phosphorus single crystal is associated with a superconducting transition, we performed alternating-current (*ac*) susceptibility measurements down to 4 K. As shown in Fig. 3a, remarkable diamagnetic throws are shown for pressures ranging from 10.4 GPa (where the zero resistance is found) to 37.3 GPa, confirming the superconductivity. The superconducting transition is also supported by our measurements under applied magnetic field, as shown in Fig. 3b. The pressure-induced structural phase and superconducting phase transitions observed in our samples are consistent with earlier reports [19, 23, 25].

We summarize our experimental results on black phosphorus in a pressure-temperature phase diagram (Fig.4a). This phase diagram includes information about the structural phase transitions and the superconducting transitions. To learn more about the anomalous *T*c vs. pressure behavior observed, we next carried out high pressure studies on the superconductivity of black phosphorus through Hall effect measurements. The corresponding Hall effect data can be found in Fig. 4b. From the perspective of overall electronic behavior, there are three distinct regions in this phase diagram: a semiconducting phase, a semimetal phase and a superconducting phase. Orthorhombic black phosphorus undergoes a transition from a semiconducting state to a semimetal state on increasing the pressure to a critical pressure (P_{C1}) of ~2.2 GPa. When the pressure is higher than ~5 GPa, the orthorhombic (O) form partially converts to the rhombohedral (R) form, as described above, (Fig.1b and Fig.S1 of the Supplementary Material [47]) and superconductivity simultaneously appears, indicating that the superconductivity is induced by the O-R structural phase transition. Since the O-R transition is sluggish, the two phases coexist

until 8.7 GPa. At a pressure of ~12.4 GPa, black phosphorus transforms to the C phase, and the superconducting transition temperature T_C shows a jump at the R-C transformation. Upon increasing pressure, T_C decreases, reaching a minimum at ~ 18.8 GPa in the C phase, and then increases again with further elevating pressure, forming a valley in the *Tc* vs. pressure behavior. A previous study on powdered black phosphorus also found such a superconducting valley in the cubic phase [25], but the physics behind that observation was not clear.

To understand the pressure-induced changes of the superconducting transition temperature in black phosphorus, we performed high-pressure Hall resistance measurements by sweeping the magnetic field (B) from 0 T to 7 T perpendicular to the *ab* plane of a single crystal sample at 15 K (close to the superconducting transition temperature) as shown in Fig. 5. We also derived the Hall coefficient (R_H) from the Hall resistance R_{xy} for each pressure point and established the pressure dependence of R_H (Fig.4b). It is noted that the sign of R_{xy} is the same as that of R_H [47]; thus the correlation between superconductivity and dominant electron- or hole-carriers can be established. In the orthorhombic semiconducting phase, the value of Hall resistance R_{xy} (or R_H) is positive, reflecting the dominance of hole-carriers in this pressure range, but R_{xy} becomes negative below a magnetic field of 3.6 T at 2.3 GPa (Fig.5b). On further pressurization, we find that $R_{xy}(B)$ completely reverses to a negative slope in the range between 2.9 GPa and 7.8 GPa (Fig 5b), and, unexpectedly, that it changes its slope again, this time from negative to positive, in the pressure range of 9.6 GPa-10.9 GPa, where black phosphorus fully enters the R phase (Fig.5c, and Fig.1b). At the pressure of ~12.4 GPa, where black P converts to the C phase, $R_{xy}(B)$ or R_H is negative (Fig.5c and Fig.4b). At 17.0 GPa, R_{xy} is almost zero below 2 T, above which the slope of $R_{xy}(B)$ increases further upon elevating field up to 23.4 GPa and then decreases

with further increasing pressure (as indicated by arrows in Fig.5d). This complicated variation of Hall resistance and Hall coefficient with pressure implies that the topology of the Fermi surface of black phosphorus undergoes substantial changes in the pressure range investigated.

In the mixed phase (O+R phase) region, $R_{xy}(B)$ of black phosphorus displays non-linearity (Fig.5b), though R_H is overall negative, and thus the data imply that there exist two types of carriers (electrons and holes) at the Fermi surface. The negative R_H observed in the range of the O+R mixed phase demonstrates that the electron carriers are dominant. However, R_H becomes positive when black phosphorus transforms to a single R phase (Fig.4b). Interestingly, $R_{xy}(B)$ of the R phase presents linear behavior for magnetic fields below 7 T (Fig.5c). These results suggest that only one type of hole-carrier is found in the R form [48]. Since the absolute value of the negative R_H detected from the mixed phase is much higher than that of the positive R_H observed in the single R phase (Fig.4b), it can be concluded that the electron-carriers detected in the mixed phase region are mainly contributed by the non-superconducting orthorhombic phase. The results observed both in the R phase and the mixed O+R phase in the pressurized phosphorus imply that hole-carriers play an important role in developing superconductivity. Moreover, we find that the superconducting T_C in the R phase increases as the population of the hole-carriers increases, indicating that higher concentrations of hole-carriers favor higher superconducting T_Cs in the R phase.

At pressures of ~12 GPa, black phosphorus converts from the R phase to the C phase. The superconducting T_C shows a jump at this pressure (Fig.4a). Simultaneously, R_H changes its sign from positive to negative again (Fig.4b). Our R_{xy} measurements demonstrate that the linear slope of $R_{xy}(B)$ is no longer present at P> 12 GPa (Fig.5c),

and that a non-linear R_{xy} with respect to B is found in the C phase (12-50 GPa), indicating again the coexistence of electron and hole carriers. Significantly, within the single C phase regime, the sign of $R_H(P)$ changes from negative to positive at P_{C2} (~17 GPa), near the pressure where the valley (*i.e.* the minimum value) of the superconducting transition temperature is observed (Fig.4a and 4b). This sign change of R_H with pressure in a single superconducting material in the absence of a structural phase transition implies a pressure-induced Lifshitz transition in the simple cubic elemental phosphorus. We thus suggest that the relative population change between hole and electron carriers results in a reconstruction of the Fermi surface [5, 8, 49, 50]. Electronic structure calculations on cubic black phosphorus indicate that there are both large and small Fermi surfaces near the Fermi energy [51-53] and further that the electronic structure at specific places in the Brillion zone is particularly sensitive to the size changes of unit cell size in the pressure regime where the valley in the superconducting *Tc* vs. pressure is observed [28,54], as revealed by our experiments on the Hall effect to be a likely scenario in this "simple" cubic main group element. It is worth pointing out that the valley in T_C at 18.8 GPa is probably the result of competing mechanism that may include electronic as well as phononic effects. The connection between the reconstruction of the Fermi topology around the transition point and the corresponding change of electron-phonon coupling deserves further investigation.

In summary, our superconducting *Tc* vs. -pressure phase diagram together with the evolution of structure and Hall coefficient provide insight into the importance of hole-carriers in developing superconductivity and enhancing T_C in pressurized black phosphorus. Our results demonstrate that, when hole-carriers become dominant in the rhombohedral or cubic phases, in the former the superconductivity emerges and in the

latter the superconducting T_C is enhanced. Further, we interpret our data to indicate that the puzzling T_C vs. pressure valley in simple cubic phosphorus is a consequence of a reconstruction of the Fermi surface (a Lifshitz transition) leading to a change in dominant carrier type. These results provide new fundamental information not only for shedding light on the physics of superconductivity in non-metallic elements that are transformed into metals but also for understanding the important role of hole-carriers in developing superconductivity in complex systems.

ACKNOWLEDGEMENTS

The authors would like to thank Prof. Zhongxian Zhao for stimulating discussions. The work in China was supported by the National Key Research and Development Program of China (Grant No. 2017YFA0302900, 2016YFA0300300 and 2017YFA0303103), the NSF of China (Grants No. 91321207, No. 11427805, No. U1532267, No. 11604376), the Strategic Priority Research Program (B) of the Chinese Academy of Sciences (Grant No. XDB07020300). The work at Princeton was supported by the Gordon and Betty Moore Foundation EPiQS initiative, grant GBMF-4412.

REFERENCES AND NOTES

1. H. Liu, Y. Du, Y. Deng, and D. Y. Peide, *Chem. Soc. Rev.* **44**, 2732 (2015).
2. E. S. Reich, *Nature* **506**, 19 (2014).
3. W. Lu, H. Nan, J. Hong, Y. Chen, C. Zhu, Z. Liang, X. Ma, Z. Ni, C. Jin, and Z. Zhang, *Nano Res.* **7**, 853 (2014).

4. Q. Wu, L. Shen, M. Yang, Y. Cai, Z. Huang, and Y. P. Feng, *Phys. Rev. B* **92**, 035436 (2015).
5. Z. Xiang, G. Ye, C. Shang, B. Lei, N. Wang, K. Yang, D. Liu, F. Meng, X. Luo, and L. Zou, *Phys. Rev. Lett.* **115**, 186403 (2015).
6. K. Akiba, A. Miyake, Y. Akahama, K. Matsubayashi, Y. Uwatoko, H. Arai, Y. Fuseya, and M. Tokunaga, *J. Phys. Soc. Jpn.* **84**, 073708 (2015).
7. J. Zhao, R. Yu, H. Weng, and Z. Fang, *Phys. Rev. B* **94**, 195104 (2016).
8. P. L. Gong, D. Y. Liu, K. S. Yang, Z. J. Xiang, X. H. Chen, Z. Zeng, S. Q. Shen, and L. J. Zou, *Phys. Rev. B* **93**, 195434 (2016).
9. C. H. Li, Y. J. Long, L. X. Zhao, L. Shan, Z. A. Ren, J. Z. Zhao, H. M. Weng, X. Dai, Z. Fang, and C. Ren, *Phys. Rev. B* **95**, 125417 (2017).
10. H. Liu, A. T. Neal, Z. Zhu, Z. Luo, X. Xu, D. Tománek, and D. Y. Peide, *ACS Nano* **8**, 4033 (2014).
11. L. Li, Y. Yu, G. J. Ye, Q. Ge, X. Ou, H. Wu, D. Feng, X. H. Chen, and Y. Zhang, *Nat. Nanotech.* **9**, 372-377 (2014).
12. F. Xia, H. Wang, and Y. Jia, *Nat. Commun.* **5**, 4458 (2014).
13. L. Cartz, S. Srinivasa, R. Riedner, J. Jorgensen, and T. Worlton, *J. Chem. Phys.* **71**, 1718 (1979).
14. K. Shimizu, T. Kimura, S. Furomoto, and K. Takeda, *Nature* **412**, 316 (2001).
15. J. S. Schilling, *Frontiers of high pressure research II: Application of high pressure to low-dimensional novel electronic materials*. pp. 345-360, (2001).
16. A. S. Sefat, *Rep. Prog. Phys.* **74**, 124502 (2011).

17. A. Rodin, A. Carvalho, and A. C. Neto, *Phys. Rev. Lett.* **112**, 176801 (2014).

18. J. Hamlin, *Physica C* **514**, 59 (2015).

19. T. Kikegawa and H. Iwasaki, *Acta. Cryst. B* **39**, 158-164 (1983).

20. I. Shirotani, A. Fukizawa, H. Kawamura, T. Yagi, and S. Akimoto, *Solid State Physics Under Pressure, Terra Scientific Publishing Company,* p207-211 (1985).

21. I. Shirotani, H. Kawamura, K. Tsuji, K. Tsuburaya, O. Shimomura, and K. Tachikawa, *Bull. Chem. Soc. Jpn.* **61**, 211 (1988).

22. I. Shirotani, K. Tsuji, M. Imai, H. Kawamura, O. Shimomura, T. Kikegawa, and T. Nakajima, *Phys. Lett. A* **144**, 102 (1990).

23. Y. Akahama, M. Kobayashi, and H. Kawamura, *Phys. Rev. B* **59**, 8520 (1999).

24. S. M. Clark and J. M. Zaug, *Phys. Rev. B* **82**, 134111 (2010).

25. J. Wittig, B. Bireckoven, and T. Weidlich, *Solid State Physics Under Pressure, Terra Scientific Publishing Company*, p217-222 (1985).

26. H. Kawamura, I. Shirotani, and K. Tachikawa, *Solid State Commun.* **54,** 775 (1985).

27. M. Karuzawa, M. Ishizuka, and S. Endo, *J. Phys.: Condens. Matter* **14,** 10759 (2002).

28. J.A. Flores-Livas, A. Sanna, A. P. Drozdov, L. Boeri, G. Profeta, M. Eremets, and S. Goedecker, *Phys. Rev. Mater.* **1**, 024802 (2017).

29. T. Yamauchi, K. Shimizu, N. Takeshita, M. Ishizuka, K. Amaya, and S. Endo, *J. Phys. Soc. Jpn.* **63**, 3207 (1994).

30. M. Norman and C. Pepin, *Rep. Prog. Phys.* **66**, 1547 (2003).

31. C. Buzea and K. Robbie, *Supercon. Sci. Technol.* **18**, R1 (2004).

32. I. I. Mazin, *Nature* **464**, 183 (2010).

33. J. Paglione and R. L. Greene, *Nat. Phys.* **6**, 645 (2010).

34. S. He, J. He, W. Zhang, L. Zhao, D. Liu, X. Liu, D. Mou, Y.-B. Ou, Q.-Y. Wang, and Z. Li, *Nat. Mater.* **12**, 605 (2013).

35. B. Keimer, S. Kivelson, M. Norman, S. Uchida, and J. Zaanen, *Nature* **518**, 179 (2015).

36. I. Kikoin and B. Lasarew, *Nature* **129**, 57 (1932).

37. J. Hirsch and J. Hamlin, *Physica C* **470**, S937 (2010).

38. G. Webb, F. Marsiglio, and J. Hirsch, *Physica C* **514**, 17 (2015).

39. J. Hirsch, *High-Tc Copper Oxide Superconductors and Related Novel Materials*. pp. 99-115, 2017.

40. S. Lange, P. Schmidt, and T. Nilges, *lnorg. Chem.* **46**, 4028 (2007).

41. T. Matsuoka, and K. Shimizu, *Nature* **458,** 186 (2009).

42. L. J. Van der Pauw, *Philips Tech. Rev.* **20**, 220 (1958).

43. L. Sun, X. J. Chen, J. Guo, P. Gao, Q. Z. Huang, H. Wang, M. Fang, X. Chen, G. Chen, Q. Wu, C. Zhang, D. Gu, X. Dong, L. Wang, K. Yang, A. Li, X. Dai, H. K. Mao, and Z. Z. Zhao, *Nature* **483**, 67 (2012).

44. M. Debessai, T. Matsuoka, J. Hamlin, J. Schilling, and K. Shimizu, *Phys. Rev. Lett.* **102**, 197002 (2009).

45. H. Mao, J. A. Xu, and P. Bell, *J. Geophys. Res.* **91**, 4673-4676 (1986).

46. A. Brown, and S. Rundqvist, *Acta Crystallogr.* **19**, 684 (1965).

47. See Supplemental Material at [ ] for sample measurements.

48. Y. Luo, H. Chen, J. Dai, Z.-a. Xu, and J. D. Thompson, *Phys. Rev. B* **91**, 075130 (2015).

49. C. Liu, T. Kondo, R. M. Fernandes, A. D. Palczewski, E. D. Mun, N. Ni, A. N. Thaler, A. Bostwick, E. Rotenberg, and J. Schmalian, *Nat. Phys.* **6**, 419 (2010).

50. D. F. Kang, Y. Z. Zhou, W. Yi, C. L. Yang, J. G, Y. G Shi, S. Zhang, Z. Wang, C. Zhang, S. Jiang, A. G. Li, K. Yang, Q. Wu, G. M. Zhang, L. L. Sun, and Z. X. Zhao, *Nat. Commun.* **6**, 7804 (2015).

51. D.-K. Seo and R. Hoffmann, *J. Sol. St. Chem.* **147**, 26 (1999).

52. M. Rajagopalan, M. Alouani, and N. Christensen, *J. Low Temp. Phys*. **75**, 1 (1989).

53. T. Sasaki, K. Shindo, K. Niizeki, and A. Morita, *Solid State Commun.* **62**, 795-799 (1987).

54. Wu, X. X. *et al.* Is electron-phone coupling enough to explain superconductivity in simple cubic phosphorus? (to be published).

Footnote: The pressure of the S-M transition in this study is ~1 GPa higher than that previously reported in Ref 16. The discrepancy may originate in the distinct crystal growth methods employed. The single crystal samples used in the current study were grown by an ambient-pressure catalyzed vapor transport technique (see methods), while the samples reported in Ref. 16 were synthesized under high pressures and temperatures. Our comparison of the Hall coefficient (R_H) of samples prepared by

these different methods found that the R_H (~17.2 cm^3/C) of the sample synthesized by the high-pressure high-temperature method is much lower than that (92 cm^3/C) of our sample when subjected to ~ 0.7 GPa. Thus, it is reasonable that the semiconductor-to-semiconductor transition for our sample needs *higher* pressure due to its lower carrier density.

AUTHOR INFORMATION

†Corresponding author

llsun@iphy.ac.cn

* These authors contributed equally to this work.

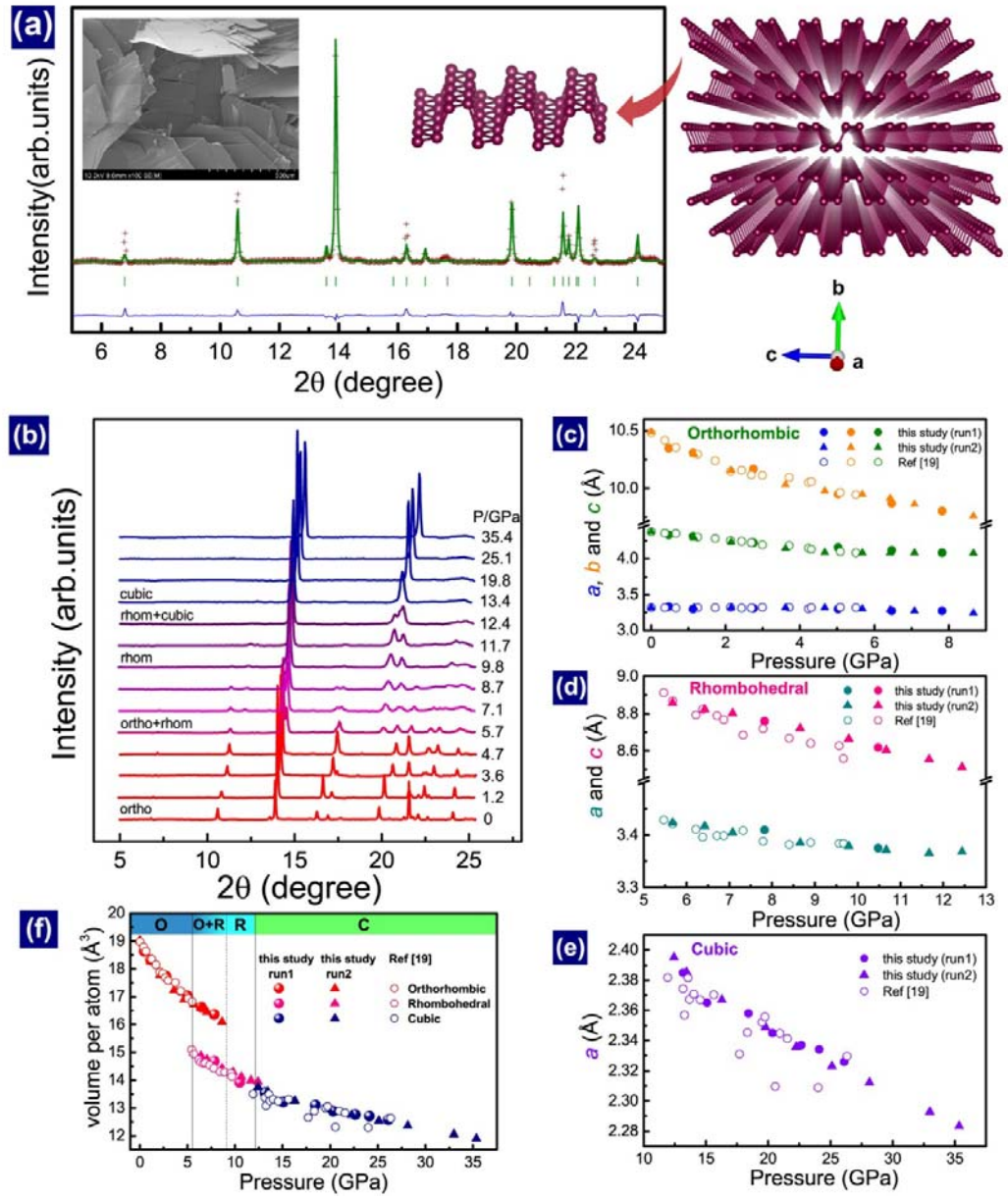

Figure 1 Structural information for black phosphorus at ambient pressure and high pressure. (a) Experimental, indexed X-ray diffraction patterns of black phosphorus at ambient pressure. The red crosses represent experimental data, and the green line and bars represent the calculated peak positions for the orthorhombic phase. The left inset is a scanning electron microscope (SEM) image of the as-grown black

phosphorus single crystals. The right upper figure shows the crystal structure of orthorhombic black phosphorus. (b) Powder X-ray diffraction patterns of black phosphorus at different pressures (X-ray wavelength = 0.6199 Å), showing three structure phases up to 35 GPa. (c)-(e) Lattice parameters versus pressure in the orthorhombic (O), rhombohedral (R) and simple cubic (C) phases. (f) Pressure dependence of the atomic volume of black phosphorus.

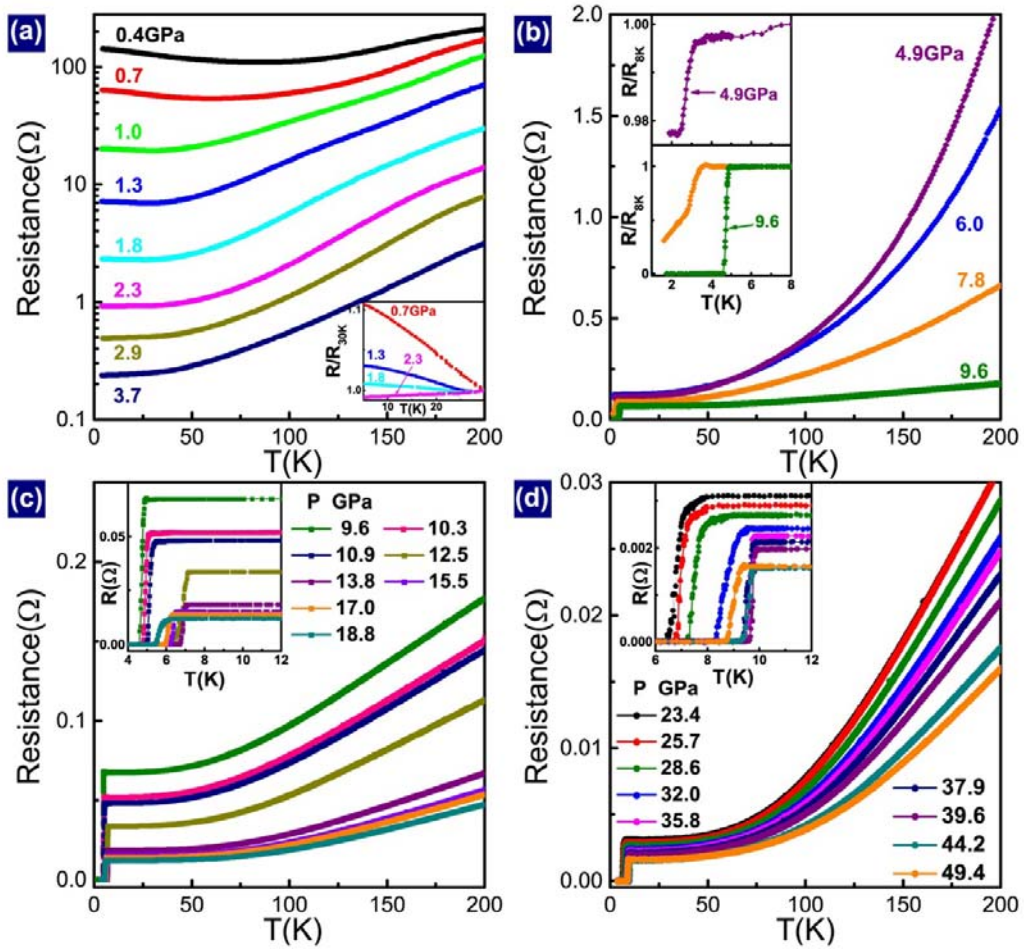

Figure 2 Electrical resistances at different pressures. (a) - (d) Electrical resistance as a function of temperature for single crystal black phosphorus at different pressures.

The insets display enlarged views of the resistance or normalized resistance in the lower temperature range around the superconducting transition.

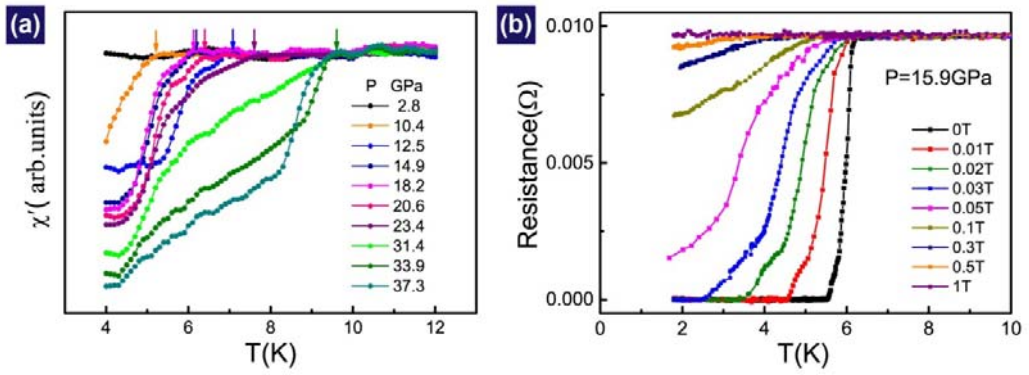

Figure 3 Diamagnetism of pressurized Black P single crystals. (a) The real part of the alternating-current susceptibility (χ') as a function of temperature at different pressures. The arrows denote the onset temperatures of the superconducting transitions. (b) Temperature dependence of electrical resistance of black P under different magnetic fields at 15.9 GPa.

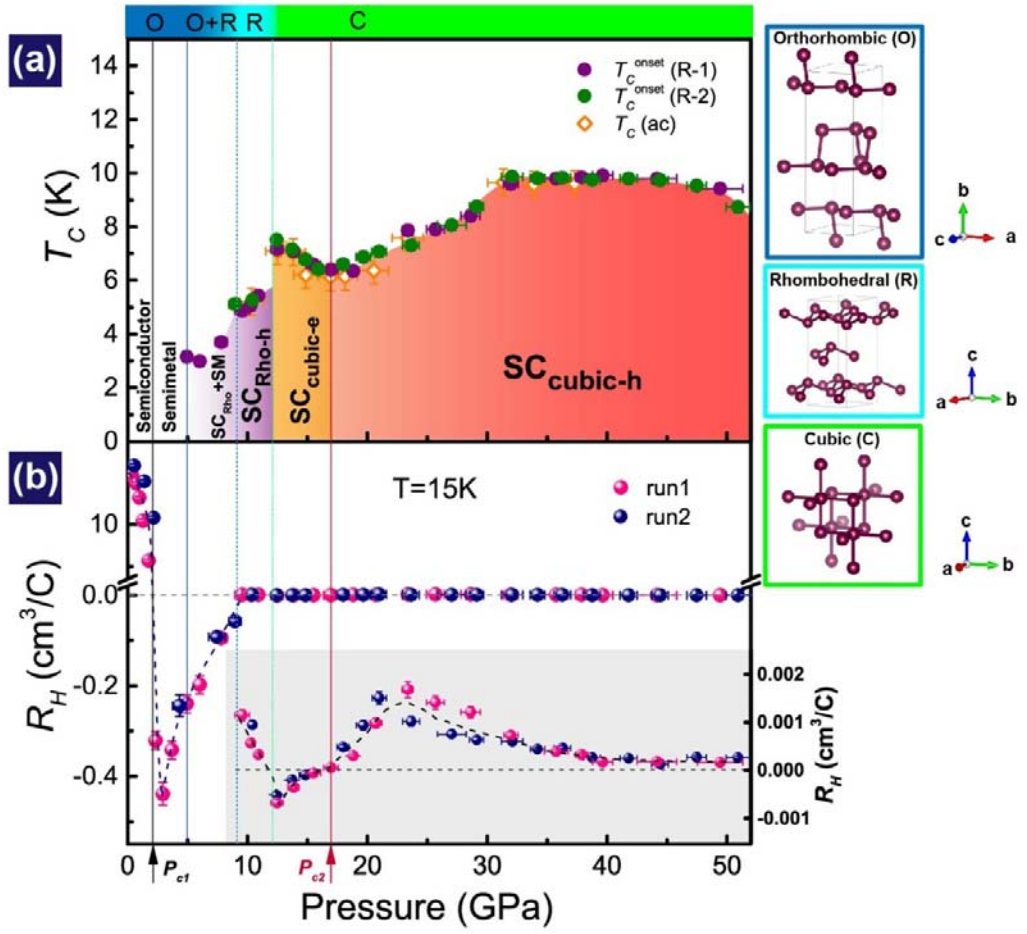

Figure 4 Structural, superconducting and Hall coefficient (R_H) phase diagram of black phosphorus at different pressures. (a) Pressure-Temperature phase diagram combined with structural phase information. Here SM and SC_{Rho-h} represent semimetal and superconducting phases with rhombohedral structure and dominant hole-carriers, respectively. $SC_{cubic-e}$ and $SC_{cubic-h}$ stand for superconducting phase with cubic structure and dominance of electron-carriers and hole-carriers, respectively. T_C^{onset} (*R*-1) and T_C^{onset} (*R-2*) represent the onset temperature of superconducting transitions determined from resistance measurements for run-1 and run-2. T_C (*ac*) represents the superconducting transition temperature determined by *ac* susceptibility measurements. (b) Pressure dependent R_H measured at 15K. The inset displays the

detailed changes of R_H at the structural phase transition boundaries. The pink and blue solid points represent Hall coefficients obtained from two independent runs. P_{c1} and P_{c2} stand for the critical pressures of the Lifshitz transitions.

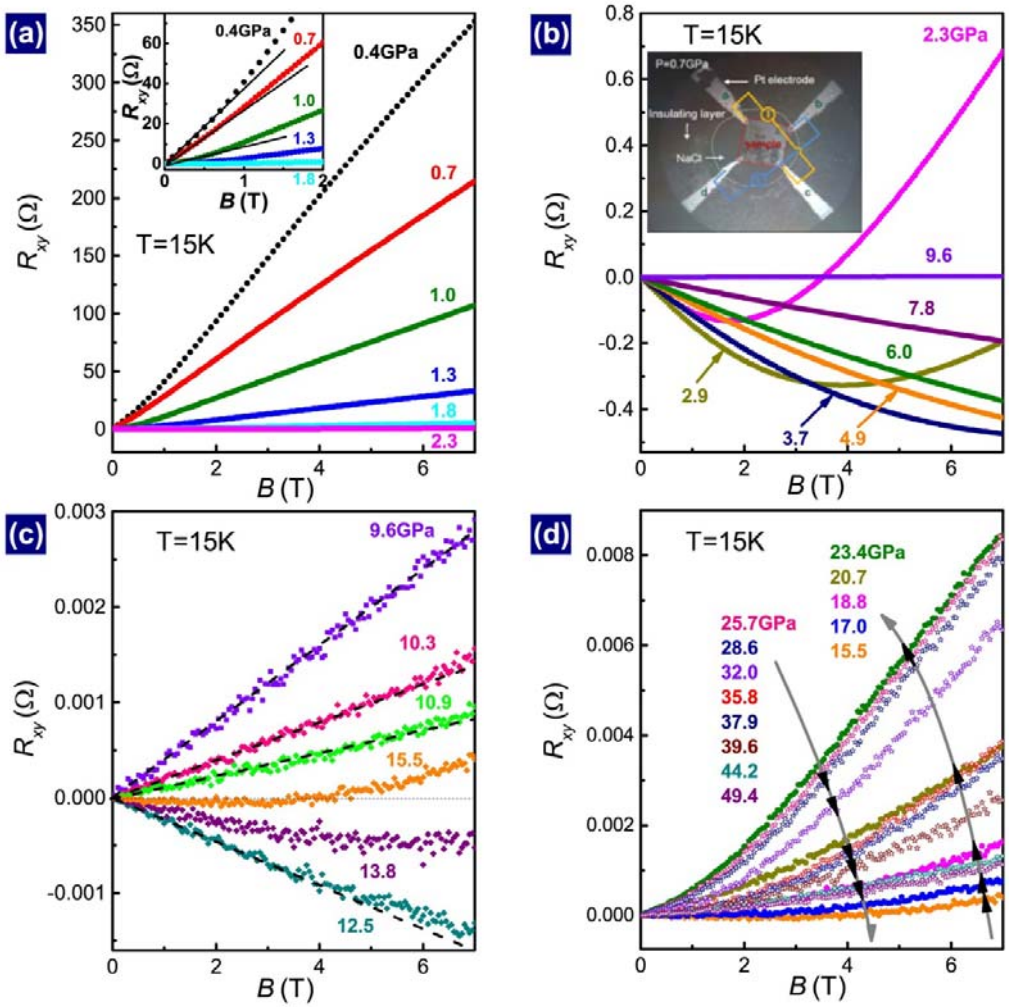

Figure 5 Hall resistance (R_{xy}) versus magnetic field (B) at 15 K and different pressures for black phosphorus single crystals. Plots of R_H-B in the pressure range of (a) 0.4 GPa-2.3 GPa, (b) 2.3 GPa - 9.6 GPa, (c) 9.6 GPa -15.5 GPa and (d) 15.5 GPa - 49.4 GPa. The inset of the figure 5b displays the top view of the sample and the arrangements of electrode for our high-pressure Hall measurements in a diamond anvil cell. The red square represents the black phosphorus single crystal and the four

white dash triangles on the corners of the sample show the contact areas of the electrodes.